Soft Matter

ARTICLE

Probing the Dynamic Self-Assembly Behaviour of Photoswitchable Wormlike Micelles in Real Time

Elaine A. Kelly,[a] Judith E. Houston[b] and Rachel C. Evans*[c]

Received 00th January 20xx,
Accepted 00th January 20xx

DOI: 10.1039/x0xx00000x

www.rsc.org/

Understanding the dynamic self-assembly behaviour of azobenzene photosurfactants (AzoPS) is crucial to advance their use in controlled release applications such as drug delivery and micellar catalysis. Currently, their behaviour in the equilibrium *cis*- and *trans*-photostationary states is more widely understood than during the photoisomerisation process itself. Here, we investigate the time-dependent self-assembly of the different photoisomers of a model neutral AzoPS, tetraethylene glycol mono(4',4-octyloxy,octyl-azobenzene) ($C_8AzoOC_8E_4$) using small-angle neutron scattering (SANS). We show that the incorporation of *in-situ* UV-Vis absorption spectroscopy with SANS allows the scattering profile, and hence micelle shape, to be correlated with the extent of photoisomerisation in real-time. It was observed that $C_8AzoOC_8E_4$ could switch between wormlike micelles (*trans* native state) and fractal aggregates (under UV light), with changes in the self-assembled structure arising concurrently with changes in the absorption spectrum. Wormlike micelles could be recovered within 60 seconds of blue light illumination. To the best of our knowledge, this is the first time the degree of AzoPS photoisomerisation has been tracked *in-situ* through combined UV-Vis absorption spectroscopy-SANS measurements. This technique could be widely used to gain mechanistic and kinetic insights into light-dependent processes that are reliant on self-assembly.

Introduction

It has long been known that the self-assembly properties of surfactants can be tuned by adjusting the pH, temperature and salinity of the solution.[1–3] A more attractive way to alter the self-assembly is to simultaneously modulate both the polarity and geometry of the surfactant by incorporation of a light-sensitive moiety in the structure.[1] Such optical manipulation is advantageous as it allows a system with a constant chemical composition to be maintained, without additives. Light offers several benefits such as good spatial and temporal resolution, as well as tuneable wavelength and intensity.

Azobenzene is the preferred light-responsive chromophore as its photoisomerisation is robust and fully reversible, without any photochemical side reactions such as dimerisation or scission.[4] Azobenzene photosurfactants (AzoPS) combine the physicochemical properties (surface activity, micelle formation *etc.*) of surfactants with the light-responsivity of azobenzene. Rapid isomerisation between *trans*- and *cis*-forms results in different polarities and geometries for each isomer.[5,6] This variation in the properties upon exposure to light has been used to destabilise photofoams on demand[7] and to reversibly change the flow characteristics in a microfluidic device.[8] Several fundamental trends have been established: (1) upon irradiation with UV light, AzoPS can form predominantly *cis* photostationary states (PSS) in good yield.[4] (2) An assembly of majority *trans*-isomers can be recovered with blue light irradiation, with an assembly of 100% *trans*-isomers only being attainable *via* thermal relaxation.[6,9] UV-Vis absorption spectroscopy is a powerful tool to track the photoisomerisation process and characterise the proportion of *cis*- and *trans*-isomers in solution, as each presents a different optical fingerprint.[9,10] (3) The *cis*-form, owing to its increased polarity, also has a higher critical micelle concentration (CMC) than the *trans*-isomer.[11]

As AzoPS become increasingly used in emerging technologies,[12–15] it is crucial that their dynamic self-assembly behaviour under photoisomerisation be understood. However, while the self-assembly behaviour of the *cis*- and *trans*-PSS at equilibrium has been reported for several AzoPS structures,[16–19] few studies follow the isomerisation process and self-assembly changes *in-situ*. Tabor *et al.* used time-resolved (TR)-SANS to track the structural changes of three carbohydrate-based AzoPS over time.[20] They observed that upon UV irradiation, and depending on the concentration regime, either a total loss of micellar structure, a decrease in aggregation number or a change in the micellar dimensions can occur. Lund *et al.* used TR-small-angle X-ray scattering to study the kinetics of micelle dissolution and reformation of the cationic AzoPS, AzoTMA, (4-butyl-4'-(3-trimethylammoniumpropoxy)-phenylazobenzene) at concentrations close to the CMC.[21] It was found that AzoTMA could transition between monomers and aggregates in

[a] School of Chemistry and CRANN, University of Dublin, Trinity College, College Green, Dublin 2, Ireland.
[b] Jülich Centre for Neutron Science (JCNS-4), Forschungszentrum Jülich GmbH, Lichtenbergstr. 1 85748 Garching, Germany.
[c] Department of Materials Science and Metallurgy, University of Cambridge, 27 Charles Babbage Road, Cambridge, CB3 0FS, U.K.
Electronic Supplementary Information (ESI) available: instrumentation, synthesis and characterisation, photostability of azobenzene cycling, photoisomerisation studies, SANS data and model fitting, calculation of the packing parameter. See DOI: 10.1039/x0xx00000x

timescales of less than a few seconds, without the formation of premicellar clusters.

Neutral AzoPS structures are less investigated compared to their cationic counterparts and have been used in fewer applications.[4,22] However, they have the benefit of a lower CMC, as well as being suitable for applications where a charged surfactant is undesirable. Here, we investigate the light-dependent self-assembly of a simple, neutral tetraethylene glycol AzoPS, tetraethylene glycol mono(4',4-octlyloxy, octyl-azobenzene) ($C_8AzoOC_8E_4$, Figure 1a) around the CMC. We integrate *in-situ* UV-Vis absorption spectroscopy with SANS to determine the extent of photoisomerisation in real time. By correlating this knowledge to the scattering profile we gain an understanding of the dynamic changes in the micellar structure as a result of photoisomerisation. To the best of our knowledge this is the first study of AzoPS to employ *in-situ* UV-Vis absorption spectroscopy for SANS measurements.

Experimental

Materials

Tetraethylene glycol mono(4',4-octlyloxy, octyl-azobenzene) ($C_8AzoOC_8E_4$) was synthesised following a slight modification of previously reported literature procedures.[23,24] A detailed description of the synthetic procedure and structural characterisation can be found in the Electronic Supplementary Information (ESI).

Methods

Ex-situ UV-Vis absorption spectra were recorded on a Perkin Elmer Lambda 35 spectrometer with a slit width of 0.5 nm. Measurements were carried out in quartz cells with a 1 cm path length.

The experimental set-up for simultaneous UV-Vis absorption-SANS measurements is shown in Figure 1b. The device setup includes an Ocean Optics FX UV-Vis spectrometer with preconfigured wavelength range of 200-850 nm, 25 µm slits and lenses for enhanced sensitivity, Ocean Optics DH-2000-DUV lamp with shutter (190-2500 nm) and Oceanview software. Fibre optic cables were positioned perpendicular to the direction of the neutron beam. The cell holder was adapted from an Ocean Optics adjustable collimating lens holder. For light irradiation, high power, mounted light emitting diodes (LEDs), blue (36.4 µW, 450 nm) and ultraviolet (57.7 µW, 365 nm) were purchased from Thorlabs, Inc.

Small-angle neutron scattering experiments were performed using the KWS-2 instrument in the Jülich Centre for Neutron Science (JCNS) at the Heinz Maier Leibnitz Zentrum (MLZ) in Garching, Germany.[25] The measurements were performed using sample-to-detector distances of 2, 8 and 20 m and a neutron λ of 5 Å ($\Delta\lambda/\lambda$ = 10%), to optimise the q-range of 0.002-0.4 $Å^{-1}$ and the beam flux. These data were converted to absolute scale (cm^{-1}) through reference to the scattering from a secondary standard sample (Plexiglas).

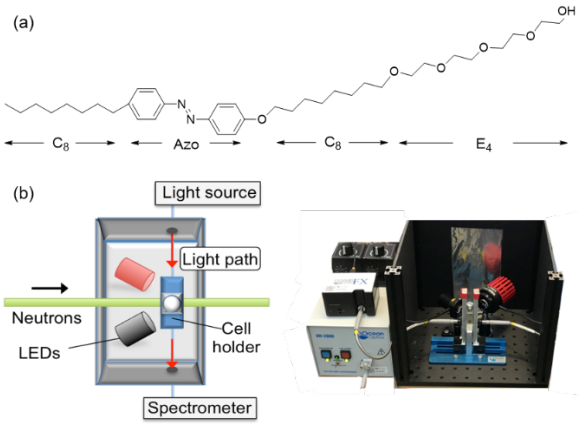

Figure 1. (a) Molecular structure of the AzoPS, $C_8AzoOC_8E_4$. (b) Schematic overview and photograph of the setup used for an *in-situ* UV-Vis absorption spectroscopy-SANS experiment with LED (UV or blue) light irradiation.

Static measurements were performed on each sample before irradiation with UV light (*trans*-dominant native state), under UV light (*cis*-dominant state) and under blue light (the recovered *trans*-dominant state).

Time-resolved scattering profiles and UV-Vis absorption spectra were collected under irradiation with UV light and blue light for the *trans-cis* and *cis-trans* isomerisation processes, respectively. Each isomerisation took 10-15 min. SANS data were initially recorded over 15 s intervals and combined post-measurement into 60 s intervals. The scattering patterns were averaged over at least 5 cycles to improve statistics. *In-situ* UV-Vis absorption spectra were recorded every second. UV-Vis spectra were compared across each SANS averaging cycle to ensure no deterioration of the sample had occurred. It was found that the final absorption spectrum, after several hours of photoisomerisation cycles, was identical to the initial one (Figure S1, ESI). Due to the high absorption coefficient of the AzoPS (ε = 12,300 L mol^{-1} cm^{-1}), sample concentrations were limited to 0.2 mM to avoid saturation of the detector.

SANS Data Modelling. Wormlike micelles (WLM) are typically characterised in terms of their contour length, L, Kuhn length, b, and cross-sectional radius, R_{CS} (Figure 2).

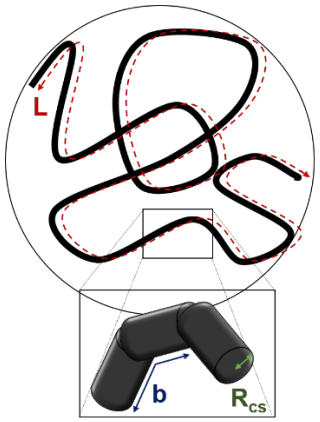

Figure 2. Schematic representation of a wormlike micelle and its associated physical parameters: contour length, L, Kuhn length, b, and cross-sectional radius, R_{CS}.

The scattering function, (S(q, L ,b)), of a semi-flexible chain with a uniform scattering length density and elliptical cross-section, taking excluded volume effects into account, is used here to fit the scattering profiles of WLM and is given by:[26,27]

$$S(q,L,b) = [1 - w(qR_g)S_{Debye}(q,L,b) + f_{corr}(q)w(qR_g)[1.22(qR_g)^{\frac{-1}{0.585}} + 0.4288(qR_g)^{-\frac{2}{0.585}} - 1.651(qR_g)^{\frac{-3}{0.585}}] + \frac{Cn_b}{n_b}\{\frac{4}{15} + \frac{7}{15u} - \left(\frac{11}{15} + \frac{7}{15u}\right) \times e^{-u(q,L,b)}\} \quad (1)$$

where w(qR_g) is an empirical crossover function, n_b = L/b and f_{corr}(q) is a correction factor added by Chen *et al.* to correct unphysical errors occurring at certain L/b ratios.[27] Further details of f_{corr}(q), w(qR_g), S_{Debye}(q, L, b) and u(q, L, b) can be found in the work of Pederson *et al.*[26] and Chen *et al.*[27] This form factor is normalised by particle volume, averaging over all possible orientations of the flexible cylinder.

Provided that the length scales of L and R_{CS} are well-separated, the high q scattering intensity from the cylindrical cross-section of the WLM can be separated from that of the semi-flexible wormlike chain as given by:[28]

$$< P(q,c) >= P_{WC}(q,L(c),b)P_{CS}(q,R_{CS}) \quad (2)$$

where <P(q, c)> is the full micellar form factor, c is the concentration, P_{WC} is a form factor, in this case, S(q, L, b), used to fit the semi-flexible chain as outlined above in Eq. 1, and P_{CS} is the form factor describing the cross-sectional radius of the WLM. Analysis of the scattering intensity in the high q region can be separated out in this manner as the local cylindrical cross-section is generally unaltered with changing surfactant concentration (WLM tend to grow 1D along their length) and inter-micellar interactions are also screened on this local level. P_{CS}(q) is described by an elliptical cylinder model in this work, with a scattering intensity given by:[29,30]

$$\boldsymbol{I(q) = \frac{1}{v}\int d\psi \int d\phi \int d\rho(\theta,\phi,\psi)F^2(q,\alpha,\psi)\sin(\theta)\, d\theta} \quad (3)$$

where:

$$\mathrm{F}(q,\alpha,\psi) = 2\frac{J_1(x)\sin(y)}{xy} \quad (4)$$

and

$$x = q\sin(\alpha)[r_{major}^2 sin^2(\psi) + r_{minor}^2\cos(\psi)]^{\frac{1}{2}}; y = \frac{L}{2}qcos(\alpha) \quad (5)$$

θ and ϕ define the orientation of the axis of the cylinder, ψ and α define the orientation of the major axis of the ellipse with respect to the vector q, J_1 is the Bessel function of first order and r is the cylinder radius.

The scattering from fractal-like aggregates was modelled according the following equation:[31]

$$I(q) = \phi V_{block}(\rho_{block} - \rho_{solvent})^2 P(q)S(q) + bkg \quad (6)$$

where in this case, ϕ represents the volume fraction of the spherical building block particles comprising the fractal-like aggregate, V_{block} is the volume of a single building block, ρ_{block} and $\rho_{solv.}$ are the scattering length densities of the spherical building blocks and solvent, respectively. P(q) and S(q) are the scattering from the randomly distributed spherical blocks and the interference from such blocks arranged in fractal-like aggregates (Equations 7-9).

$$P(q) = F(qR_0)^2 \quad (7)$$

$$\boldsymbol{F(qR_0) = 3[\sin(qR_0) - qR_0cos(qR_0)]/(qR_0)^3} \quad (8)$$

$$\boldsymbol{S(q) = 1 + \frac{D_f\Gamma(D_f-1)}{[1+\frac{1}{(q\xi)^2}]^{(D_f-1)/2}}\frac{\sin[(D_f-1)\tan^{-1}(q\xi)]}{(qR_0)^{D_f}}} \quad (9)$$

where ζ is the correlation length, R_0 is the radius of the building block, Γ(x) is the gamma function of argument x, and D_F represents the fractal dimension. All model fittings were carried out using the SASview 4.0.1 software.[30]

Results and discussion

Central to the ability to relate the self-assembly behaviour of AzoPS to the extent of photoisomerisation in real-time is the existence of different optical fingerprints for the *cis*- and *trans*-isomers. Figure 3 shows the UV-Vis absorption spectra of C_8AzoOC$_8$E$_4$ (0.065 mmol L^{-1}) in both the *cis*- and *trans*-PSS, and the native *trans*-form. The more thermodynamically stable *trans*-isomer (by ~50 kJ mol^{-1})[6] can be recognised from the π→π* band at 332 nm. Photoisomerisation to the *cis*-isomer upon UV irradiation is confirmed by a change of the π→π* absorption wavelength from 332 to 308 nm, with a concurrent decrease in intensity, along with the appearance of a new absorption band (n→π*) at 445 nm.[9] The degree of isomerisation from *trans* to *cis* C_8AzoOC$_8$E$_4$ is 61% (Eq. S1, ESI). The *trans*-isomer can be recovered by irradiation with blue light, yielding an assembly of 90% *trans*-isomers.

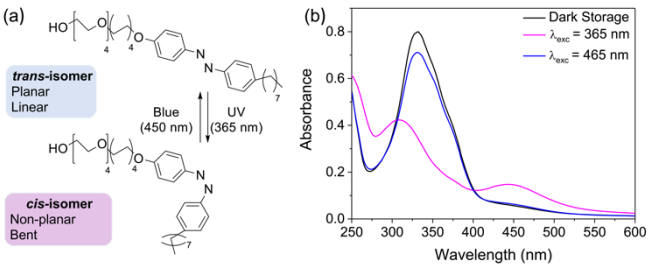

Figure 3. C_8AzoOC$_8$E$_4$ isomerises between *cis*- and *trans*-forms upon irradiation with UV or blue light, respectively, with each having a characteristic absorbance spectrum. (a) Chemical structures of the *cis*- and *trans*-isomers (b) UV-Vis absorption spectra of C_8AzoOC$_8$E$_4$ (0.065 mmol L^{-1} in H_2O) under UV (pink line) and blue (blue line) irradiation and after storage in the dark (black line).

The scattering profiles and corresponding absorption spectra obtained from combined *in-situ* UV-Vis absorption spectroscopy and SANS measurements of C_8AzoOC$_8$E$_4$ (0.2 mmol L^{-1}) are shown in Figures 4 and 5. This concentration was

chosen to maximise the scattering count rate, without exceeding the maximum absorbance possible for UV-Vis absorbance spectroscopy. This concentration is above the CMC of both the *cis*- and *trans*-states (CMC_{trans} = 0.11 mmol L^{-1}; CMC_{cis} = 0.13 mmol L^{-1}) with $C_8AzoOC_8E_4$ appearing fully soluble at this concentration.

$C_8AzoOC_8E_4$ initially presents a scattering profile characteristic of wormlike micelles, with varying slopes for the decay across the entire *q* range (Figure 4a). This assignment is supported by the rheological behaviour of the surfactant. $C_8AzoOC_8E_4$ was found to have a high viscosity and exhibited non-Newtonian shear-thinning behaviour (Figure S9, ESI). This is consistent with the formation of wormlike micelles.[32–34] These asymptotic regions correspond to the different length scales of the physical parameters of the WLM (*L*, *b*, R_{CS}). At low *q* the scattering profile is distinguished by the self-avoiding random walk of the semi-flexible chain, characterised by a decay of approximately q^{-2}.[26,28] In the mid *q*-region (~0.011 $Å^{-1}$), where shorter length scales are probed, a decay of q^{-1} can be observed. This correlates to scattering of rods or cylinders, reflecting the stiffness of the wormlike chain.[26,28] Scattering at higher *q* values corresponds the local cross-section. As aforementioned, the scattering from the cross-sectional radius at high *q* can be separated from that of lower *q*. The bottom scattering profile in Figure 4a (60 s UV irradiation) is fit in this manner, by deconvoluting the data into two contributions, one from the overall semi-flexible chain of the WLM (flexible elliptical cylinder model fitted from 0.002 – 0.1 $Å^{-1}$) and one corresponding to the more rigid constituent cylinders (elliptical cylinder model fitted from 0.1 – 0.35 $Å^{-1}$). This approach could be used for the first three scattering profiles (60 - 180 s of UV illumination), after which a transition to a fractal-like aggregate was observed (Figure 4b). With increasing UV irradiation time, the q^{-1} region at ~0.011 $Å^{-1}$ diminishes, ultimately resulting in a smooth decrease in scattering intensity that decays as $q^{-2.6}$ in the low- and mid-*q* regions from 420 seconds onwards. q^n scalings with $2 > n > 3$ in this region are commonly ascribed to fractal aggregates.[31] Due to the transitionary nature of these scattering profiles, these fits are cautiously assigned and the physical parameters resulting from them will not be discussed in detail. (Table S2, ESI) The intermediate scattering profiles at 240 and 300 s could not be well described by either the WLM or fractal model fitting approaches, suggesting that the most significant micellar rearrangements occur within this time frame. The analogous SANS plots in terms of absolute scattering intensity are available in the Supporting Information (Figure S3, ESI).

The observed changes in the micelle structure correspond well with changes in the UV-Vis absorption spectra, where the π→π* band decreases in intensity during the first 180 s of irradiation, blue-shifts during 240–300 s irradiation, before finally maintaining intensity and wavelength from 360 s onwards. This implies that there is no significant lag time, and that variations in the aggregate structure arise concurrently with molecular isomerisation. The photoisomerisation reaction follows first order kinetics (Figure 3c, inset) with a rate constant of 8.6 × 10^{-3} s^{-1}, as commonly observed for azobenzene systems.[12,23,35] This implies that the AzoPS solution was not so strongly absorbing as to result in diffusion-limited photoisomerisation kinetics, as has been reported in some cases.[20]

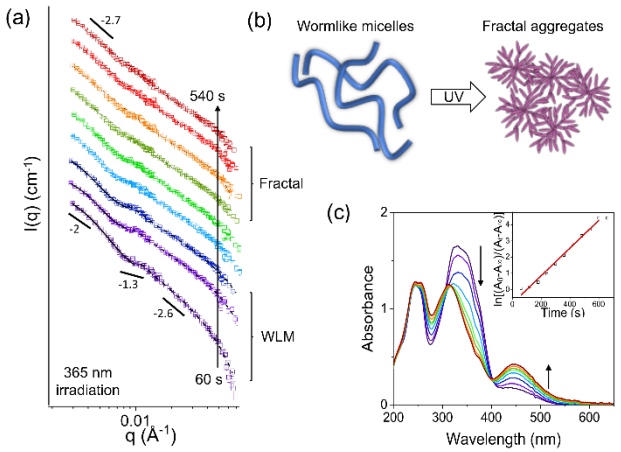

Figure 4. Self-assembly behaviour of $C_8AzoOC_8E_4$ in D_2O (0.2 mmol L^{-1}) upon *trans-cis* photoisomerisation. (a) SANS scattering profiles as a function of UV irradiation time. $C_8AzoOC_8E_4$ transitions from wormlike micelles to fractal-like aggregates. Fits to the flexible elliptical cylinder model are indicated by a solid black line, the elliptical cylinder model by a dashed line and fractal model by a dotted line. The scattering curves have been offset for clarity. The solid black lines indicate the slopes in each *q* regime. (b) Schematic representation of the wormlike micelle to fractal aggregate transition. (c) *In-situ* UV-Vis absorption spectra upon UV-irradiation. Inset shows the first order reaction kinetics associated with the photoisomerisation.

The scattering profiles and corresponding absorption spectra for the reverse isomerisation under blue light are shown in Figure 5. $C_8AzoOC_8E_4$ was found to form WLMs in all cases. With increasing irradiation time, $C_8AzoOC_8E_4$ transitions from long ribbon-like WLMs to WLMs consisting of elliptical cylinders of a lower eccentricity (Table S1, ESI). This development is marked by a change in the low *q* slope from q^{-2} to $q^{-1.8}$ and from 240 s onwards, a return of the plateau at ~0.011 $Å^{-1}$. As this plateau becomes more pronounced, deconvolution of the scattering profile into fits from two model contributions, as previously outlined, is required. The analogous SANS plots in terms of absolute scattering intensity are available in the Supporting Information (Figure S4, ESI).

It is apparent that changes to the self-assembled AzoPS structure occur quite rapidly, with variations in the scattering profiles occurring on the same time-scale as changes in the UV-Vis absorption spectra. Despite the similarity of the first scattering profile in Figure 5a (60 s, blue light) with the final one of Figure 4a (540 s, UV light), a flexible elliptical cylinder model was inadequate to describe the former scattering profile (Figure S3, ESI). This indicates that after only 60 s of illumination with blue light, the majority *cis*-AzoPS solution can be returned to WLM. The *cis-trans* photoisomerisation reaction also follows first-order kinetics, with a rate constant of 4.7 × 10^{-3} s^{-1} (Figure 4c, inset). No further changes to the absorption spectra are observed after 540 s of either UV or blue light irradiation, indicating that the *cis*- and *trans*-PSS are reached. The degree of isomerisation was found to be 58% and 86% for the *cis*- and *trans*-PSS respectively (Figure S2, ESI). These values are in good

agreement with those obtained previously from static measurements at concentrations below the CMC (Figure 3b).

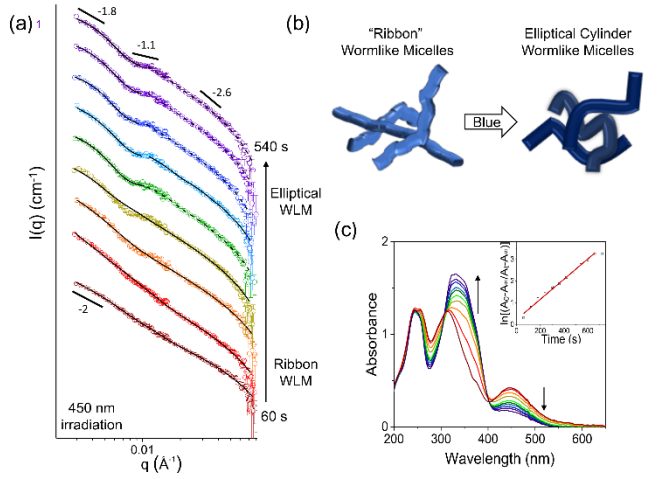

Figure 5. Self-assembly behaviour of $C_8AzoOC_8E_4$ in D_2O (0.2 mmol L^{-1}) upon *cis-trans* photoisomerisation. (a) SANS scattering profiles as a function of blue irradiation time. $C_8AzoOC_8E_4$ transitions from ribbonlike wormlike micelles to elliptical cylinder wormlike micelles. Fits to the flexible elliptical cylinder model are indicated by a solid black line and to the elliptical cylinder model by a dashed line. The scattering curves have been offset for clarity. (b) Schematic representation of the wormlike micelle transition. (c) *in-situ* UV-Vis absorption spectra upon UV-irradiation. Inset shows that reverse isomerisation also proceeds *via* first reaction order kinetics.

The changes in the self-assembled structure upon photoisomerisation can be explained by the difference in polarity and geometry between *trans*- and *cis*-isomers. *Cis*-azobenzene incorporates a kink in the otherwise linear $C_8AzoOC_8E_4$ structure, disrupting its ability to form WLM. There are some fundamental similarities between WLM and fractal aggregates. WLM are treated as a semi-flexible chain consisting of many locally rigid cylinders. Likewise, fractals can be considered as comprised of many self-similar constituent parts. The packing parameter, *P*, for $C_8AzoOC_8E_4$ is 0.42 (Section 6, ESI), with values of $1/3 < P < 1/2$ being typical for the formation of cylinders.[36,37] It appears that $C_8AzoOC_8E_4$ has a preference to self-assemble into cylindrical aggregates, which, upon incorporation of a "bent" azobenzene core (and the associated change in polarity), prefer to manifest themselves as fractals rather than wormlike micelles. This is further supported by the fact that the scattering intensities are on the same order under both illumination conditions. (Figure S4, ESI). Due to the difference in CMC between *cis*- and *trans*-isomers it would be expected for more monomers to be present for the assemblies formed under UV light compared to under blue light. As the scattering intensity remains roughly similar it can be concluded that the effective size of the scattering bodies is comparable for both the WLM and fractal aggregates.[38]

The degree of isomerisation can be used to explain this behaviour. As only 58% *cis*-isomers are formed upon photoisomerisation, it does not take long to return to a majority *trans*-isomer state and preferential WLM formation (60 s blue irradiation, 53% *trans*-isomers.). Similarly, the number of *cis*-monomers in solution would be expected to be quite small compared to a solution with a higher degree of isomerisation. This is striking as photoisomerisation can therefore be considered as only a minor disruption to the AzoPS solution, but also significant enough to completely change the morphology of the micellar aggregates. This highlights the sensitivity of the self-assembly process to changes in the delicate hydrophobic-hydrophilic balance and geometry of the molecule. The trends observed here were found to persist at equilibrium (Figure S5, ESI) and at higher $C_8AzoOC_8E_4$ concentrations of 1 mM (Figure S6, ESI), with WLM and fractal aggregates detected for the *trans*- and *cis*-PSS, respectively.

Conclusions

In this study we have shown using a model AzoPS, $C_8AzoOC_8E_4$, that the integration of UV-Vis absorption spectroscopy with SANS measurements can provide mechanistic and kinetic insights into its photoisomerisation and self-assembled structure. Combining these techniques in this way allows the dynamic behaviour of the surfactant, which is often over-looked, to be emphasised. Upon irradiation with UV light, $C_8AzoOC_8E_4$ undergoes a wormlike micelle to fractal transition at concentrations above the CMC in D_2O. This is a promising result as single component photoswitchable wormlike micelle systems are rarely reported, with smart wormlike micelle systems having vast potential as on-demand rheology modifiers.[39,40] Wormlike micelles could be recovered with as little as 60 s of blue irradiation (36.4 µW), with extended illumination times resulting in WLMs of a lower cylindrical eccentricity. This study also highlights the robustness of the azobenzene chromophore. It was found that the AzoPS could reversibly cycle between *cis*- and *trans*-isomers without deterioration over several hours. This combined UV-Vis/SANS approach could be extended to many other systems to allow monitoring of their self-assembly process, as the only requirement is the presence of a characteristic absorption spectrum. This technique would be of particular value to dynamic, non-equilibrium processes such as the controlled release of small molecules from self-assembled aggregates, *e.g.* drug delivery, micellar catalysis.

Conflicts of interest

There are no conflicts of interest to declare.

Acknowledgements

This work is based upon experiments performed at the KWS-2 instrument operated by JCNS at the Heinz Maier-Leibnitz Zentrum (MLZ), Garching, Germany. EAK thanks the Irish Research Council for a Government of Ireland postgraduate scholarship. This work was supported in part by an Isaac Newton Trust/University of Cambridge Early Career Support Scheme grant. This work benefited from the use of the SasView application, originally developed under NSF award DMR-0520547. SasView also contains code developed with funding from the European Union's Horizon 2020 research and

innovation programme under the SINE2020 project, grant agreement No. 654000.

Notes and references

1 P. Brown, C. P. Butts and J. Eastoe, *Soft Matter*, 2013, **9**, 2365–2374.
2 C. Rosslee and Abbo, *Curr. Opin. Colloid Interface Sci.*, 2000, 81–87.
3 X. Liu and N. L. Abbott, *J. Colloid Interface Sci.*, 2009, **339**, 1–18.
4 J. Eastoe and A. Vesperinas, *Soft Matter*, 2005, **1**, 338.
5 G. S. Hartley, *J. Chem. Soc.*, 1938, 633–642.
6 K. G. Yager and C. J. Barrett, *J. Photochem. Photobiol. A Chem.*, 2006, **182**, 250–261.
7 E. Chevallier, C. Monteux, F. Lequeux and C. Tribet, *Langmuir*, 2012, **28**, 2308–2312.
8 D. Baigl, *Lab Chip*, 2012, **12**, 3637.
9 H. M. Dhammika Bandara and S. C. Burdette, *Chem. Soc. Rev.*, 2012, 1809–1825.
10 I. K. Lednev, T. Ye, P. Matousek, M. Towrie, P. Foggi and F. V. R. Neuwahl, *Chem. Phys. Lett.*, 1998, 68–74.
11 S. Shinkai, K. Matsuo, A. Harada and O. Manabe, *J. Chem. Soc. Perkins Trans*, 1982, 1260–1265.
12 E. Chevallier, A. Mamane, H. A. Stone, C. Tribet, F. Lequeux and C. Monteux, *Soft Matter*, 2011, **7**, 7866.
13 A. Diguet, R. M. Guillermic, N. Magome, A. Saint-Jalmes, Y. Chen, K. Yoshikawa and D. Baigl, *Angew. Chem. Int. Ed.*, 2009, **48**, 9281–9284.
14 C. T. Lee, K. A. Smith and T. A. Hatton, *Biochemistry*, 2005, **44**, 524–536.
15 S. Chen, W. Zhang, C. Wang and S. Sun, *Green Chem.*, 2016, **18**, 3972–3980.
16 T. Shang, K. A. Smith and T. A. Hatton, *Langmuir*, 2006, **22**, 1436–1442.
17 S. Peng, Q. Guo, P. G. Hartley and T. C. Hughes, *J. Mater. Chem. C*, 2014, **2**, 8303–8312.
18 S. Peng, Q. Guo, T. C. Hughes and P. G. Hartley, *Langmuir*, 2014, **30**, 866–872.
19 C. Blayo, J. E. Houston, S. M. King and R. C. Evans, *Langmuir*, 2018, **34**, acs.langmuir.8b02109.
20 R. F. Tabor, M. J. Pottage, C. J. Garvey and B. L. Wilkinson, *Chem. Commun.*, 2015, **51**, 5509–5512.
21 R. Lund, G. Brun, E. Chevallier, T. Narayanan and C. Tribet, *Langmuir*, 2016, **32**, 2539–2548.
22 S. Santer, *J. Phys. D. Appl. Phys.*, , DOI:10.1088/1361-6463/aa95ca.
23 T. Shang, K. A. Smith and T. A. Hatton, *Langmuir*, 2003, 10764–10773.
24 R. F. Tabor, R. J. Oakley, J. Eastoe, C. F. J. Faul, I. Grillo and R. K. Heenan, *Soft Matter*, 2009, **5**, 78–80.
25 A. Radulescu, V. Pipich, H. Frielinghaus and M.- Appavou, *J. Phys. Conf. Ser.*, 2012, **351**, 012026.
26 J. S. Pedersen and P. Schurtenberger, *Macromolecules*, 1996, **29**, 7602–7612.
27 W. R. Chen, P. D. Butler and L. J. Magid, *Langmuir*, 2006, **22**, 6539–6548.
28 C. A. Dreiss, *Soft Matter*, 2007, **3**, 956–970.
29 L. . Feigin and D. . Svergun, *Structure Analysis by Small Angle X-ray and Neutron Scattering*, Plenum, New York, 1987.
30 *http://www.sasview.org/*, accessed 05/18.
31 J. Teixeira, *J. Appl. Crystallogr.*, 1988, **21**, 781–785.
32 T. M. McCoy, A. Valiakhmetova, M. J. Pottage, C. J. Garvey, L. De Campo, C. Rehm, D. A. Kuryashov and R. F. Tabor, *Langmuir*, 2016, **32**, 12423–12433.
33 H. Oh, A. M. Ketner, R. Heymann, E. Kesselman, D. Danino, D. E. Falvey and S. R. Raghavan, *Soft Matter*, 2013, **9**, 5025–5033.
34 J. Wang, Y. Feng, N. R. Agrawal and S. R. Raghavan, *Phys. Chem. Chem. Phys.*, 2017, **19**, 24458–24466.
35 B. A. Cicciarelli and K. A. Smith, *Langmuir*, 2007, 4753–4764.
36 J. N. Israelachvili, D. J. Mitchell and B. W. Ninham, *J. Chem. Soc. Faraday Trans.,* 1975, 1525–1568.
37 Y. Takahashi, M. Kishimoto and Y. Kondo, *J. Colloid Interface Sci.*, 2016, **470**, 250–256.
38 C. T. Lee, K. A. Smith and T. Alan Hatton, *Langmuir*, 2009, **25**, 13784–13794.
39 B. Song, Y. Hu and J. Zhao, *J. Colloid Interface Sci.*, 2009, **333**, 820–822.
40 Z. Chu, C. A. Dreiss and Y. Feng, *Chem. Soc. Rev.*, 2013, **42**, 7174.